Monte Carlo intrinsic surfaces and density profiles for liquid surfaces

P. Tarazona[1] and E. Chacón[2]
[1]*Departamento de Física Teórica de la Materia Condensada, and Instituto Nicolás Cabrera, Universidad Autónoma de Madrid, E-28049 Madrid, Spain*
[2]*Instituto de Ciencia de Materiales de Madrid, Consejo Superior de Investigaciones Científicas. Cantoblanco, E-28049 Madrid, Spain*
(Received 31 May 2004; revised manuscript received 9 September 2004; published 6 December 2004)

Operational definitions for the intrinsic surface to be used in computer simulations of liquid surfaces are discussed and tested along with Monte Carlo simulations of simple liquid models. The results are contrasted with the theoretical framework of the capillary wave theory (CWT), and with the strongly structured intrinsic profiles used in the interpretation of x-ray reflectivity experiments for cold liquid metals. The definition of a minimal area intrinsic surface pinned to a set of pivot atoms at the surface leads to intrinsic density profiles with the sharpest atomic resolution, but which are beyond the assumption of the CWT, with strong correlations between the intrinsic profiles and the fluctuations of the intrinsic surface and with an effective wave-vector-dependent surface tension.

DOI: 10.1103/PhysRevB.70.235407 PACS number(s): 68.03.Hj, 68.03.Kn, 61.30.Hn

I. INTRODUCTION

In 1893 van der Waals[1,2] pioneered the description of the liquid-vapor interface through a smooth density profile $\rho(z)$. The present experimental and theoretical techniques[2,3] give us a much enhanced microscopic resolution for $\rho(z)$, but at the same time unveil the problem of its statistical interpretation. Unless pinned by external fields, a free liquid surface is statistically delocalized by long wavelength capillary waves (CW's)[4]; the one-molecule density distribution $\rho(z)$ would be smoothed, up to missing any signature of the interface, while the two-molecule distribution would develop long-ranged transverse correlations. The Earth's gravity localizes the liquid surfaces within a few molecular diameters σ and damps the transverse correlations beyond millimeter distances,[5] but still leaves them well outside the usual microscopic approaches. The sharper density profiles observed experimentally for cold liquids[6] result from the combined effect of the sample size (including the curvature of the liquid drops) and the size of the measurement transverse window, which limit the role of the CW and introduce the dependence of the density profile on the transverse sampling area A_0. In computer simulations the typical transverse area is much smaller than the experimental windows and finite-size effects have been observed in the interfacial width[2,7] and in the layering structures.[8]

Capillary wave theory (CWT) (Refs. 4, 5, 9, and 10) provides the framework to introduce the surface fluctuations and the size dependence of the density profiles by means of an intrinsic surface $z=\xi(\mathbf{R})$, with $\mathbf{R}=(x,y)$ representing the instantaneous microscopic boundary between the vapor and the liquid phases. Thus, in computer simulations of a liquid slab, with the center of mass on the $z=0$ plane and two liquid-vapor interfaces parallel to it, the intrinsic surface is described through its Fourier components

$$\xi(\mathbf{R}) = \sum_{\mathbf{q}} \hat{\xi}_q e^{i\mathbf{q}\cdot\mathbf{R}}, \tag{1}$$

with the sum over transverse wave vectors $\mathbf{q}=2\pi(n_x,n_y)/L_x$ and $n_x,n_y=0,\pm1,\pm2\ldots$, to include the periodic boundary conditions on the transverse direction (with $L_x=L_y\equiv A_0^{1/2}$). The fixed number of particles N and the low compressibility of the bulk liquid would limit the fluctuations of the $|\mathbf{q}|=0$ component $\hat{\xi}_0$ around its mean value

$$\langle\hat{\xi}_0\rangle \approx \pm \frac{N - L_z\rho_v}{2(\rho_l-\rho_v)A_0}. \tag{2}$$

The $\pm$ sign gives the upper/lower Gibbs dividing surface, defined in terms of the coexisting liquid (ρ_l) and vapor (ρ_v) densities. With the exception of checking the statistical independence and equivalence of the two surfaces on the slab, we will refer to them as a single surface in order to avoid the cumbersome labeling of upper and lower Fourier components $\hat{\xi}_q$.

The lower wave vector cutoff $q_l=2\pi/L_x$ for the CW fluctuations of the intrinsic surface creates a transverse size L_x dependence of the density profile

$$\rho(z,L_x) \equiv \left\langle \frac{1}{A_0}\sum_{i=1}^{N}\delta(z-z_i)\right\rangle, \tag{3}$$

where the angular brackets represent the equilibrium statistical average. The intrinsic density profile defined as

$$\tilde{\rho}(z) = \left\langle \frac{1}{A_0}\sum_{i=1}^{N}\delta[z-z_i+\xi(\mathbf{R}_i)]\right\rangle, \tag{4}$$

should take out the dependence on L_x. However, the specific definition of $\xi(\mathbf{R})$ and, particularly, the upper cutoff q_u for the level of resolution at which $\xi(\mathbf{R})$ follows the molecular positions, would affect to the shape of the intrinsic profile, which we refer to as $\tilde{\rho}(z,q_u)$ whenever this q_u dependence has to be made explicit.

The first assumption of the CWT (Ref. 4) to relate the alternative descriptions of the interface given by $\rho(z,L_x)$ and $\tilde{\rho}(z,q_u)$ is that the later is statistically uncorrelated with the intrinsic surface, leading to

$$\rho(z,L_x) = \int dz' \mathcal{P}_\xi(z') \tilde{\rho}(z - z' - \langle \hat{\xi}_0 \rangle, q_u), \tag{5}$$

where $\mathcal{P}_\xi(z)$ is the probability distribution for the local fluctuations of the intrinsic surface $\xi(\mathbf{R}) - \langle \hat{\xi}_0 \rangle$. The second CWT assumption is that the fluctuations of $\xi(\mathbf{R})$ at the inverse temperature $\beta = (k_B T)^{-1}$ follow a simple surface Hamiltonian with the macroscopic surface tension γ_0. This leads to uncorrelated Gaussian probabilities for the Fourier components with mean square values $|\hat{\xi}_q|^2 = (\beta \gamma_0 A_0 q^2)^{-1}$ for any $|\mathbf{q}|$ between the lower and the upper wave vector limits and to the Gaussian probability

$$\mathcal{P}_\xi(z) = \frac{1}{\sqrt{2\pi \Delta_{CW}}} \exp\left(- \frac{z^2}{2\Delta_{CW}} \right). \tag{6}$$

The CW mean square amplitude $\Delta_{CW}(L_x, q_u) = \Sigma_q |\hat{\xi}_q|^2$, for $2\pi/L_x \leqslant |\mathbf{q}| < q_u$, provides the link between the dependence of $\rho(z,L_x)$ on the system size, and the dependence of $\tilde{\rho}(z,q_u)$ on the assumed CW upper cutoff q_u. The fluctuations of $\hat{\xi}_0$ may be easily included is that scheme as an additional *bulk* contribution Δ_b to be added to Δ_{CW}.

There is no serious doubt about the upward use of the CWT to incorporate the effects of long wavelength capillary waves. The density profile $\rho(z,L_x)$ from a computer simulation with fairly large L_x may be safely convoluted as $\tilde{\rho}(z,q_u)$ in Eq. (5), to get the density profile $\rho(z,L_x')$ with an even larger L_x', just taking the contributions of $|\hat{\xi}_q|^2$ for $2\pi/L_x' \leqslant |\mathbf{q}| < 2\pi/L_x$. However, its downward use, trying to extract a sharper view of the molecular structure at the liquid surface from $\rho(z,L_x)$ has been frustrated by the uncertainties in the value of q_u and its effects on the shape of $\tilde{\rho}(z,q_u)$.

It is expected that q_u should not go beyond $2\pi/\sigma$. This qualitative threshold has often been used to set the value of the upper cutoff, while $\tilde{\rho}(z)$ has sometimes being taken as a sharp step function,[9,11] which in Eq. (5) would give an error-function representation of $\rho(z,L_x)$. Alternatively, Mecke and Dietrich[12] have assumed that $\tilde{\rho}(z)$, without explicit dependence on q_u, could be represented by the smooth density profile $\rho(z)$ obtained within a density functional (DF) approximation, which has no explicit dependence on L_x. A related DF approach to the CW structure was pioneered by Robledo *et al.*[13] and has been explored in detail by Stecki.[14] Under the assumptions of a very smooth intrinsic profile and a generic density functional expansion up to second order, the grand-potential free energy of a corrugated interface is cast into an effective Hamiltonian for $\xi(\mathbf{R})$. The direct comparison with the results of computer simulations throws light on the difficulties associated to the upper cutoff q_u, on the need to include the higher order derivatives of $\tilde{\rho}(z)$ in the functional expansion, and on the problem of separating the surface and the bulk fluctuations, tied to the definition of $\xi(\mathbf{R})$ used in computer simulations.

On the other hand, over the last 15 years the analysis of x-ray reflectivity on liquid surfaces has made important progress towards a better characterization of their microscopic structure[3] and the CWT has become a standard theoretical framework to interpret the results. The Fresnel reflectivity, for a planar and sharp step function is diminished by the interface broadening, which may be interpreted as the CW effects on a steplike or intrinsically smoothed $\tilde{\rho}(z)$;[15] however, for liquid metals such as Hg and Ga, an increase was observed rather than decrease, over the Fresnel reflectivity.[16,17] This was interpreted as the signature of atomic layering; the uncertainty in the effective size of the experimental window (typically $L_x \sim 10^3$ Å) and in the definition of q_u may be drawn together using Δ_{CW} as a free fitting parameter and the intrinsic profiles for liquid Hg were fitted to the form

$$\tilde{\rho}(z) = \tilde{n}_0 \delta(z) + \sum_{i=1}^{\infty} \frac{\tilde{n}_i}{\sqrt{2\pi \tilde{a}_i}} \exp\left[- \frac{(z - \tilde{z}_i)^2}{2\tilde{a}_i} \right], \tag{7}$$

with the first δ-function peak giving the sharpest possible resolution for the atoms at the interface, followed by a series of broadening Gaussian peaks with structures similar to those of dense liquids near planar walls.

The qualitatively different assumptions made for the shape of the intrinsic profiles in the above commented applications of the CWT, and the uncertainty in value of the upper cutoff q_u, reflect the lack of connection between the CWT and the microscopic description of the free liquid surfaces. The development of simple models, with pairwise additive interactions and very low melting temperature,[18,19] showed that the layering of free liquid surfaces was not exclusive of the metallic bonding in Hg or Ga, but that it would be a common feature of cold liquids when not preempted by their crystallization. These models have been used in MC simulations to explore different questions related to the surface layering such as the connection with the Fisher-Widom line[20,21] and, more recently,[22] to test the operational definition of the intrinsic surface, which applied to sampling of MC configurations, gives a direct evaluation of $\tilde{\rho}(z,q_u)$, to be compared with the previously conjectured forms, as well as direct access to the statistical properties of $\xi(\mathbf{R})$, to check the validity of the CWT assumptions. The following section of this paper is a detailed account of the methods used to determine the intrinsic surface associated with each microscopic configuration of the interface, while in Secs. III and IV we present and discuss the results in the context of the classical CWT and also in relation with the analysis of x-ray reflectivity experiments. The characteristics of the NVT Monte Carlo simulations for liquids slabs are equal to those reported in previous works.[18,19,22] Most of the results correspond to 2592 particles in a rectangular box with periodic boundary conditions $L_x = L_y \approx 9\sigma$ and $L_z \approx 81\sigma$, with the liquid slab filling approximately a third of the volume. To check for finite size effects we have performed some simulations with 10 368 particles and $L_x = L_y \approx 18\sigma$. The reported results correspond to three different pair potential interactions. The Lennard-Jones (LJ) interaction and the results for the soft alkali (SA) and mercurylike (Hg) models, described in previous works, are compared with those for the well known Lennard-Jones (LJ) model, all of them truncated at $r = 2.5\sigma$. All the reported temperatures are safely above the triple point to avoid any pos-

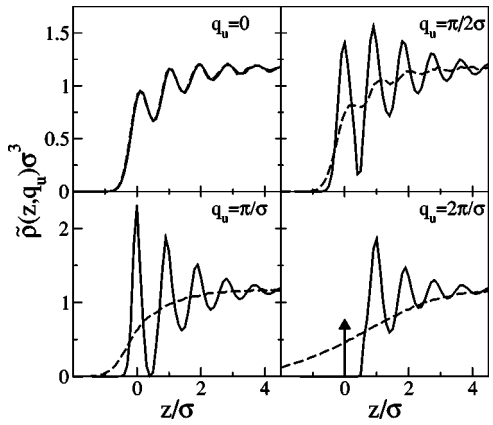

FIG. 1. Intrinsic profiles $\tilde{\rho}(z,q_u)$ in units of the atomic diameter σ for the soft-alkali model at $T/T_C=0.15$. Broken lines: the local Gibbs surface definition for the intrinsic surface. Full lines: the surface pinned definition, the arrow shows the density of the δ function layer. The upper-left corner, $q_u=0$, corresponds to the mean profile $\rho(z,L_x)$ identical for both definitions of the intrinsic surface.

sible effect of surface-induced crystallization and well below T_c to avoid the interference of bulk criticality.

II. DEFINITIONS FOR THE INTRINSIC SURFACE

A. The local Gibbs surface

The simplest operational definition of $\xi(\mathbf{R})$ would be a local generalization of the Gibbs dividing surface (2), as proposed in the early works on the CWT (Ref. 9) and recently used in computer simulations for the LJ model[14] and for polymer mixtures.[23] In our slab geometry with $L_x=L_y$ and the center of mass fixed on the $z=0$ plane, we consider the upper and lower parts of the system (particles with $z_i>0$ and $z_i<0$, respectively), and divide each subsystem in prisms of transverse size $l_x=l_y=L_x/M$, spanning a length $L_z/2$ on the normal direction. Then a piecewise intrinsic surface, with a resolution $q_u\sim 2\pi M/L_x$, is defined as

$$\xi^{(\pm)}(\mathbf{R}) = \pm \frac{N_{\pm}(\mathbf{R}) - \frac{1}{2}L_z\rho_v}{(\rho_l-\rho_v)A_0}, \tag{8}$$

where $N_{\pm}(\mathbf{R})$ is the number of particles in the prism at $\mathbf{R}$ and the sign $\pm$ corresponds to the upper and lower halves. The continuous limit of this definition is easily expressed in terms of the Fourier components

$$\hat{\xi}^{\pm}_{\mathbf{q}} = \pm \frac{1}{(\rho_l-\rho_v)A_0}\left(\sum_{\pm z_i>0} e^{-i\mathbf{q}\cdot\mathbf{R_i}} - \frac{L_z}{2}\rho_v\delta_{q,0}\right). \tag{9}$$

For $q \ll 2\pi/\sigma$, this definition of an intrinsic surface would give reasonable results, but as q approaches $2\pi/\sigma$ the mean square values $\langle|\hat{\xi}_q|^2\rangle$ grow with q, as observed by Stecki[14] in the attempt to check the extended CWT of Robledo *et al.*[13] The effect of such a behavior on the intrinsic profiles is clearly shown in the broken lines of Fig. 1 for the SA model at $T/T_c=0.15$. The upper-left corner corresponds to the density profile $\rho(z,L_x)$ or, equivalently, to the intrinsic profile (4) and (9) when q_u is below $2\pi/L_x$. The layering structure in that profile is damped with the choice of larger q_u, as shown in the other quadrants. This is due to the increasing effect of the bulk fluctuations on the position of such a Gibbsian intrinsic surface. The fluctuation in the number of molecules in a liquid prism, with base $l_x^2=(L_x/M)^2$ and spanning a height $L_z^{(l)}$, is $\langle(N-\langle N\rangle)^2\rangle = k_BT\chi_T\langle N\rangle\rho_l$, in terms of the bulk isothermal compressibility. The definition (9) for the intrinsic surface incorporates these bulk fluctuations to the position of $\xi(\mathbf{R})$ producing a mean square deviation of the local Gibbs surface

$$\Delta_b = \frac{\langle(N-\langle N\rangle)^2\rangle}{(l_x^2\rho_l)^2} \sim k_BT\chi_T L_z^{(l)} q_u^2,$$

which is not correlated to the microscopic position of the interface. With the typically low compressibility of the dense liquids, the effect of this Δ_b would be a small fraction of Δ_{CW} when used over our MC box $L_x\approx 9\sigma$, but the application to the sub-boxes increases Δ_b by a factor M^2, while Δ_{CW} decreases. The blurring of the intrinsic profiles obtained for large M (or $q_u\approx 2\pi/\sigma$) indicates that such local Gibbs dividing surface becomes fully uncorrelated with the actual position of the liquid-vapor interface. To get the highest resolution in the description of the interface through $\tilde{\rho}(z,q_u)$ we search for a different definition of $\xi(\mathbf{R})$.

B. The surface pinned definition

In our previous work[22] we proposed an operational definition of intrinsic surface, which may be carried out automatically for samplings along computer simulations. The definition uses a set of pivot atoms located at each surface of the liquid slab; to choose these pivots for a given configuration we first eliminate all the particles with less than $\nu=3$ neighbors, closer than $d=1.5\sigma$, as being in the vapor phase or forming loose hangovers on the liquid surface. Possible liquid droplets in the vapor phase are also eliminated by a cluster analysis done with the same distance d, so that all the remaining particles have ν or more neighbors in the liquid slab. At the low temperatures explored here, most of the particles belong to that class (e.g., out of the 2592 particles in our simulations only 3 or 4 are eliminated in a typical configuration of the SA model at $T/T_c=0.15$), but still it is crucial to perform this selection for the possible candidates to become surface pivots. Nevertheless, the results are quite robust with respect to the particular choice of ν and d.

The next step is to divide the liquid slab in prisms, of transverse area $l_x^2=(L_x/M)^2$, and take the most external atomic positions to form the initial sets of M^2 initial pivots, for the upper and the lower interfaces. Typically we take $M=3$, so that this procedure would give a coarse piecewise representation of $\xi(\mathbf{R})$. The limit to a smooth intrinsic surface cannot be obtained just taking a larger M, since the fluctuation effects would lead to a spurious roughness of $\xi(\mathbf{R})$, similar to that described above. Instead, we define a smooth intrinsic surface as the minimal area surface going

through all the pivots, and restricted to have only Fourier components $\hat{\xi}_q$ with $|\mathbf{q}|$ less than a maximum value q_m. In our MC simulation boxes with $L_x \approx 9\sigma$ we have typically taken $q_m = 18\pi/L_x \approx 2\pi/\sigma$. The computation of the minimal area surface is simplified if we approximate the relative difference between the area of $\xi(\mathbf{R})$ and the macroscopic area $A_0 = L_x^2$ by

$$\frac{\Delta A}{A_0} \approx \frac{1}{2}\sum_{\mathbf{q}} q^2 |\hat{\xi}_q|^2, \tag{10}$$

neglecting the contributions of order $\hat{\xi}_q^4$ and higher, as done in the CWT. A practical way to obtain the surface $z = \xi(\mathbf{R})$ going through the positions $(\mathbf{R}_j, z_j)$ for the N_p pivots, and with minimum value of Eq. (10), minimize the quadratic form

$$Q[\xi] = \sum_{j=1}^{N_p} [\xi(\mathbf{R}_j) - z_j]^2 + \epsilon \sum_{\mathbf{q}} q^2 |\hat{\xi}_q|^2, \tag{11}$$

with a very low ϵ. The degeneracy in the minimum of $Q[\xi]$ with $\epsilon = 0$ is broken by any $\epsilon > 0$, and we may take ϵ small enough to avoid the practical interference of the minimization of $\Delta A/A_0$ with the condition of $z_j = \xi(\mathbf{R}_j)$ for all the pivots, and at the same time large enough to avoid numerical problems in the resolution of the linear system. For all practical purposes $\epsilon = 10^{-6}$ or 10^{-8} give the same results.

The next step in our definition of $\xi(\mathbf{R})$ is to enlarge the number of pivots N_p, from its initial value M^2, to incorporate all those which should be considered as surface atoms. This is done by self-consistently adding as pivots all those particles which are closer than a prefixed distance τ to the surface $z = \xi(\mathbf{R})$. A new intrinsic surface is obtained through the minimization of Eq. (11) including all the new pivots, the distances of the remaining particles to this new surface are compared again with τ, and the process is iterated until there are no new additions to the list of pivots.[24] The contribution of the microscopic configuration to the intrinsic profile (4) and the statistical properties of the intrinsic surface are obtained by averaging over 10^3 to 10^4 configurations, separated at least by 50 MC steps. The right-bottom full line in Fig. 1 gives a typical example of the intrinsic profiles obtained by this procedure, compared with the results of the local Gibbs surface for the same system.

C. The parameters τ and q_m

The density profiles obtained with this intrinsic surface definition always have a first δ-function peak, as in Eq. (7), with a two-dimensional density $\hat{n}_0 = \langle N_p \rangle / A_0$, in terms of the mean number of pivots per unit area. That peak is followed by a strongly layered structure similar to that of a dense fluid near a planar wall. As shown in Fig. 2, both the value of $\hat{n}_0$ and the shape of the following structure depend on the choice of the parameter τ used to add new surface pivots in the self-consistent definition of $\xi(\mathbf{R})$. We have explored this dependence and fixed the value of τ to reduce the sensitivity with respect to it. When τ is too low the intrinsic density profiles develop shoulders just above $z = \tau$, which come from the particles which do not naturally fit in the first Gaussian

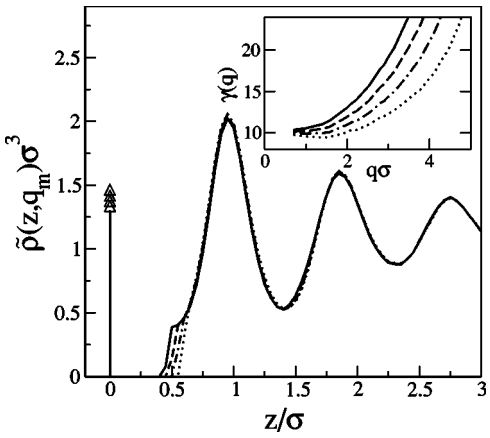

FIG. 2. Variation of the intrinsic profile $\tilde{\rho}(z, q_m)$ with respect to the choice of the parameter τ for the soft-alkali model at $T/T_c = 0.12$. Full line: $\tau = 0.46\sigma$, dashed line: $\tau = 0.50\sigma$, dashed-dotted line $\tau = 0.54\sigma$, dotted line: $\tau = 0.58\sigma$. The δ function first peaks are shown as arrows which height is the two dimensional density. The inset shows the effective q-dependent surface tension $\gamma(q)$ in $k_B T/\sigma^2$.

peak within the parametric form (7). Increasing τ incorporates these particles to the first δ-function peak, $\hat{n}_0$ grows and the shoulder decreases. However, if τ is too large there is a very rapid increase in $\hat{n}_0$, as the self-consistent determination of the pivots for some configurations grows suddenly to more than twice the value in other configurations. This is a signature that the intrinsic surface is incorporating particles which should be naturally assigned to the first inner layer, rather than to the surface, and the corrugation of $\xi(\mathbf{R})$ induced by these new pivots induces the incorporation of many others. Eventually, the number of pivots may go beyond the number of free variables in the minimization of Eq. (11) and our full procedure would fail, but even if that does not happen, the choice of τ leading to that sudden increase of $\hat{n}_0$ should be discarded. The optimal choice, reducing the shoulder at $z \approx \tau$ without blowing up the value of $\hat{n}_0$, may depend on the model and temperature, but it is always around $\tau = 0.5\sigma$, well within the intuitive meaning of this parameter to separate the intrinsic surface from the inner particles. Computationally, we have carried out in parallel the averages with different values of τ, as a good part of the computational work required to analyze a configuration with a value of τ, is saved for larger values of this parameter.

The typical value of N_p in our MC simulations with $L_x \approx 9\sigma$ is about 60, so that the maximum value of the wave vector could be reduced, well below $q_m = 18\pi/L_x$, and still have more than enough free coefficients $\hat{\xi}_{\mathbf{q}}$ to get a surface $\xi(\mathbf{R})$ going through all the pivots. However, this reduction of free variables reduces the role for the minimization of the area (10) and the corrugations of $\xi(\mathbf{R})$ increase in amplitude. That is reflected in the increase of $\langle |\hat{\xi}_q|^2 \rangle$ which reflects the over-fitting effects of forcing $\xi(\mathbf{R})$ to pass through too many pivots. If we take q_m much larger that $2\pi/\sigma$, there is an important increase in the computational work, and $\xi(\mathbf{R})$ develops unphysical wedge lines along the lines joining pivots. Although the effect on the intrinsic profiles is very small, this

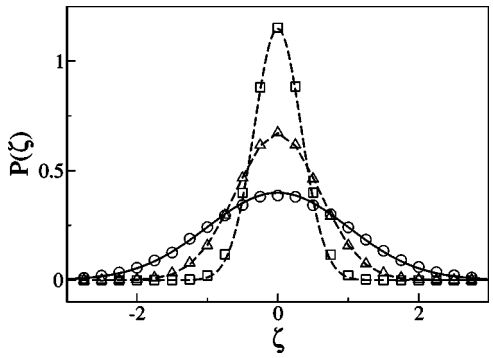

FIG. 3. Probability histograms $P(\zeta)$ of the Fourier components $\hat{\xi}_q$, normalized to the mean square prediction of the CWT $\zeta \equiv \hat{\xi}_q / \langle |\hat{\xi}_q|^2 \rangle_{\mathrm{CWT}}^{1/2}$ for the soft-alkali model at $T/T_c = 0.15$. The squares are the results for the highest value of $q = 6.2/\sigma$, the triangles for $q = 4.4/\sigma$, and the circles for the lowest value $q = 0.7/\sigma$. The broken lines are the fit to Gaussian probabilities with free width, and the full line shows the normalized width Gaussian predicted by the CWT.

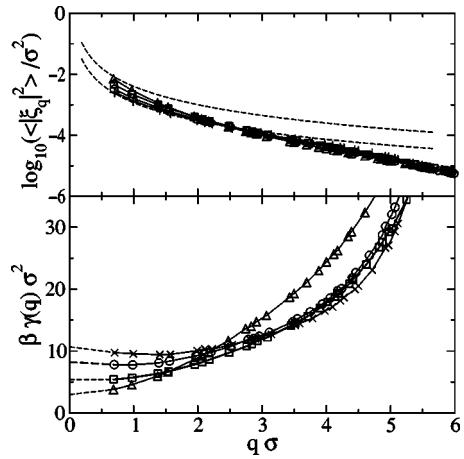

FIG. 4. The mean squared amplitude of the intrinsic surface Fourier components and the effective q-dependent surface tension $\gamma(q)$ in $k_B T$ and atomic diameter σ units, for the SA model at several temperatures. Crosses: $T/T_c = 0.12$, circles: $T/T_c = 0.15$, squares: $T/T_c = 0.21$, triangles: $T/T_c = 0.33$. The low q values of $\gamma(q)$ are extrapolated (broken lines) to the macroscopic surface tension γ_0. The dashed lines in the upper panel give the CWT predictions for $T/T_c = 0.12$ and $T/T_c = 0.33$.

tendency to form a faceted surface is reflected in the depletion of $\langle |\hat{\xi}_q|^2 \rangle$. Therefore, the natural and fairly robust choice is to take q_m near $2\pi/\sigma$.

III. STATISTICAL PROPERTIES OF THE INTRINSIC SURFACES

Along the same MC samplings used to get the intrinsic profiles we have computed the probability histograms for the Fourier components $\hat{\xi}_q$. The results in Fig. 3 correspond to the SA model at $T/T_C = 0.15$, sampled over 10^4 configurations, the amplitudes for each component are normalized to the mean squared value predicted by the CWT $\langle |\hat{\xi}_q|^2 \rangle_{\mathrm{CWT}} = (\beta \gamma_0 A_0 q^2)^{-1}$, with the macroscopic surface tension γ_0 obtained directly in previous MC simulations for the same models.[19] The probability distributions for the large $|\mathbf{q}|$ components are much narrower than the CWT prediction, but still with excellent fits to Gaussian shapes. Only for the lowest $|\mathbf{q}|$ components $\hat{\xi}_q$ do the observed distributions recover the CWT prediction represented by the full line in Fig. 3, although the slow dynamics of those long wavelength modes requires longer MC samplings to get good representations of $\mathcal{P}(\hat{\xi}_q)$. We have checked that within the precision of our sampling size, the different Fourier components are uncorrelated, and that our liquid slab is thick enough to avoid the correlations between the upper and the lower surfaces. Therefore, the statistical properties of $\xi(\mathbf{R})$ are fully described by the values of $\langle |\hat{\xi}_q|^2 \rangle$ or, equivalently, by the effective q-dependent surface tension $\gamma(q) \equiv (\beta A_0 q^2 \langle |\hat{\xi}_q|^2 \rangle)^{-1}$.

The results for $\langle |\hat{\xi}_q|^2 \rangle$ in the SA model over a wide range of temperatures are presented in Fig. 4, and compared with the CWT predictions $\langle |\hat{\xi}_q|^2 \rangle_{\mathrm{CWT}} = (\beta \gamma_0 A_0 q^2)^{-1}$ (broken lines) for the lowest and highest temperatures. Consistently with the results for $\mathcal{P}(\hat{\xi}_q)$, the observed mean squared amplitudes for the Fourier components are in good agreement with $\langle |\hat{\xi}_q|^2 \rangle_{\mathrm{CWT}}$ for the lowest wave vector q, but they fall down much faster with increasing q. This is equivalent to say that (as shown on the bottom panel of the same figure) the function $\gamma(q)$ goes to the macroscopic surface tension γ_0 for low q; but instead of the sharp threshold assumed by the CWT, with $\gamma(q) = \gamma_0$ up to an upper cutoff q_u, we get a smoothly growing effective surface tension without a well defined threshold for the CW contributions. The difference between the sharp cutoff assumed by the CWT and the gradual increase $\gamma(q) = \gamma_0 + Kq^2 + \cdots$ (in terms of a curvature energy K) has been discussed in the interpretation of x-ray reflectivity data.[25,26] Pershan[26] argued, a few years ago, that the available experimental data could not discern between these two alternatives, the second one being equivalent to the former with an effective cutoff $q_u \sim \sqrt{\gamma_0/K}$. As our results for $\gamma(q)$ grow gradually but faster than q^2, they are half way between those two assumptions, and hence they could not be directly contrasted with the experiments.

However, more recent reports on x-ray scattering by CW on several liquids[27–29] claim that the function $\gamma(q)$ may be measured, and that at low q it decreases from the $\gamma(0) = \gamma_0$ limit, reaching a minimum value well below the macroscopic surface tension, before the expected growth for large q. Such behavior had been predicted by Mecke and Dietrich,[12] from the assumptions that the equilibrium DF density profile may be used as intrinsic profile, displaced by the nominal intrinsic surface, and that the effective surface Hamiltonian might be obtained from a simple DF approximation, with dispersion interatomic potentials decaying as $1/r^6$ at large distance. According to that analysis, the minimum in $\gamma(q)$ would be produced by a singularity associated to the slow decay of the dispersion forces, so that it should not appear in our truncated LJ model, nor in the Gaussian decay model potentials.

In order to test the effects of the long-range interactions we have run a MC simulation for the untruncated LJ potential at $T/T_c=0.63$ and with $L_x \approx 9\sigma$. The intrinsic profiles are very similar for the truncated and untruncated versions of the interaction potential, and the functions $\gamma(q)$ are identical around the lower range of accessible wave vectors $q \approx 2\pi/L_x$, with small deviations of less than 5% at the higher range $q \approx 2\pi/\sigma$. The most significant change induced by the truncation of the potential comes in the macroscopic surface tension γ_0; the untruncated version of the LJ potential giving a 30% increase of γ_0 over the truncated version, within the range observed by other authors.[30] Therefore, we cannot exclude the existence of a shallow minimum in $\gamma(q)$ at $q\sigma < 0.5$, but our results would also be compatible with a monotonous growth of $\gamma(q)$. Moreover, the inset in Fig. 2 shows the dependence of $\gamma(q)$ with the choice of the parameter τ in our definition of intrinsic surface and for the largest values of τ we observe a shallow minimum in $\gamma(q)$. This corresponds to intrinsic surfaces with the highest density of surface pivots, close to the instability in our self-consistent method to select those pivot atoms, and the minimum of $\gamma(q)$ [i.e., the relative increase of $\langle|\hat{\xi}_q|^2\rangle$ over the CWT prediction $(\beta\gamma_0 A_0 q^2)^{-1}$] could be interpreted as the excess of corrugation in $\xi(\mathbf{R})$, when forced to go through too many pivots.

Therefore, the details in the definition for the intrinsic surface may change the shape of the function $\gamma(q)$ much more than the presence or absence of long-ranged interactions. Within our scheme to define $\xi(\mathbf{R})$ for each atomic configuration, the choice of the parameter τ reflects the lack of uniqueness in the definition of the intrinsic surface when q becomes comparable to the inverse atomic diameter. Different choices would share the same macroscopic limit $\gamma(q) \rightarrow \gamma_0$ for low q, but they may give different functions $\gamma(q)$ for intermediate and large q. A firm comparison with the function $\gamma(q)$ extracted from x-ray reflectivity data, could only be done through the analysis of the effective intrinsic surface measured by that technique, which would depend on the details of the experimental setup. Meanwhile, we may only rely on the aspect of the intrinsic profiles and the functions $\gamma(q)$ to select the most *natural* choice of τ for each temperature and model interaction which may hopefully be closer to an effective definition of $\xi(\mathbf{R})$ associated with the x-ray reflection on the liquid surface. For low values of τ the intrinsic profiles develop the unphysical shoulders shown by the full line in Fig. 2, and the corresponding function $\gamma(q)$ in the inset of Fig. 2 shows a rapid increase from the $q=0$ limit. Such behavior reflects the fact that we are not incorporating all the required surface pivots so the intrinsic surface is less corrugated than its natural shape and $\gamma(q)$ grows too fast. On the opposite limit, for too large values of τ, the first peak in $\tilde{\rho}(z,q_m)$, after the δ function at $z=0$, becomes very asymmetric compared with the Gaussian shape (7), with a too abrupt fall on the left side. This corresponds to the choice of too many pivot atoms, leading to an overcorrugated intrinsic surface and hence to a decreasing function $\gamma(q)$ at low q. Therefore, in the following analysis of our results we have selected those values of τ which lead to the flattest curve $\gamma(q)$ at low q, and which also happen to give the most symmetric shape

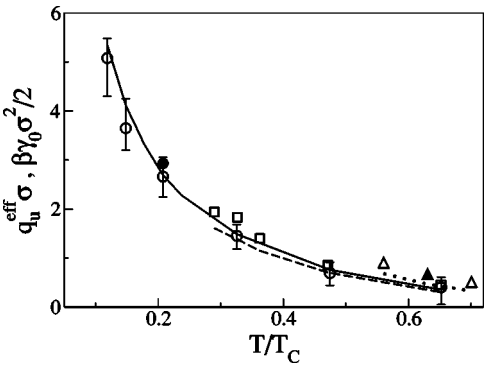

FIG. 5. The CWT-effective cutoff q_u^{eff} (circles and error bars) for the SA model over a large range of temperatures. The results for the Hg (squares) and LJ (triangles) models would have similar error bars. The lines give the values of $\beta\gamma_0\sigma^2/2$ for the three models. SA: full line, Hg: broken line, and LJ: dotted line, as functions of T/T_C. Empty symbols correspond to MC results with $N=2592$ and full symbols with $N=10\,368$.

for the second peak in $\tilde{\rho}(z,q_m)$, and use the error bars to indicate the estimated uncertainty of that natural choice. In addition to the choice of the parameter τ, directly linked to the density of selected surface pivots, there are other aspects in our intrinsic surface definition which may affect the form of $\gamma(q)$ at large q. In particular, the apparently exponential decay of $\langle|\hat{\xi}_q|^2\rangle$ at large $|\mathbf{q}|$, similar for all the models and temperatures explored here, is probably a result of the minimal surface character assumed for $\xi(\mathbf{R})$, and it may be different with other definitions. We should also be aware that the choice of τ within the above criterion becomes much more uncertain at higher temperatures; the broadening of the molecular layers in $\tilde{\rho}(z,q_m)$ with increasing T makes our definition of $\xi(\mathbf{R})$ more artificial, with the sharp threshold at $z=\tau$ to incorporate new surface pivots. Alternative definitions, based on some kind of softer threshold, should be explored to extend these studies to $T/T_c > 0.7$.

A global aspect which might be more robust with respect to the particular choice of $\xi(\mathbf{R})$ is the total mean squared amplitude of the intrinsic surface corrugation $\Delta_{CW}(L_x,q_m)$, which could be obtained from the off-specular wings in the reflectivity measurements.[26] We may define a CWT-effective cutoff q_u^{off} such that it reproduces the measured mean squared amplitude of the intrinsic surface corrugation as

$$\Delta_{CW}(L_x,q_m) \equiv \sum_{|\mathbf{q}|=q_l}^{q_m} \langle|\hat{\xi}_q|^2\rangle = \sum_{|\mathbf{q}|=q_l}^{q_u^{\text{eff}}} \frac{1}{\beta\gamma_0 A_0 q^2}. \qquad (12)$$

Interpolating within the discrete values of q imposed by the finite size, this relationship provides a value of q_u^{eff} which is independent of the box size L_x if it is large enough to reach the macroscopic limit $\gamma(q_l)=\gamma_0$ at the lower cutoff $q_l = 2\pi/L_x$. q_u^{eff} is well below our q_m and fairly independent of this parameter, since the amplitude of the modes with $q \approx 2\pi/\sigma$ is always very small. As presented in Fig. 5, the values of q_u^{eff} have a clear decay with growing temperatures, which is not blurred by the uncertainty of the choice of τ

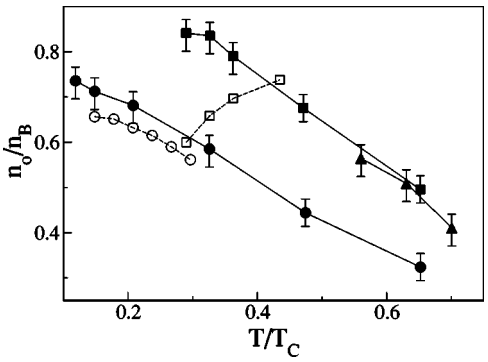

FIG. 6. Two-dimensional density of first layer n_0/n_B vs the temperature reduced to the critical one. The full symbols (and full line) show the values obtained with the present definition of intrinsic surface. The empty symbols (and dashed line) are the values of a previous work obtained fitting the simulation mean density profiles to a superposition of Gaussian layers (14). Circles, SA potential, squares: Hg potential, triangles: Lennard-Jones potential.

and, hence, it probably corresponds to a truly intrinsic characteristics of the liquid surfaces. At the low melting point of the SA model, with $T_t/T_c \approx 0.12$, we obtain $q_u^{\text{eff}} \approx 4.5/\sigma$, not far from the empirical value π/σ set in the analysis of the x-ray reflectivity data for Hg and Ga;[16,17] however, q_u^{eff} decays with T/T_c, and for the higher temperatures of the LJ liquid q_u^{eff}, it is already below the lower cutoff $q_l \approx 0.7/\sigma$ fixed by our MC box size L_x. Therefore, we have carried out some MC simulations with 10 368 particles and $L_x \approx 18\sigma$ keeping the same value of q_m and, hence, increasing the number of Fourier components used in the description of $\xi(\mathbf{R})$ by a factor 4. The extension to lower wave vectors $q_l \approx 0.35/\sigma$ requires larger sampling times, since the low q CW have a slower dynamics. The computational cost to get good statistical averages with the larger box size increases by more than a factor 20 with respect to the shorter L_x, but the resulting values of $\langle|\hat{\xi}_q|^2\rangle$ interpolate well between those obtained for the smaller MC box, and allow a better estimation of q_u^{eff}, while all the other reported properties are essentially unaffected by the size increase.

Such values of q_u^{eff} are well below the typical threshold values ($2\pi/\sigma$ or π/σ) assumed in the applications of the CWT. Moreover, we find an empirical but quite accurate relation shown by the line $\beta\gamma_0\sigma^2/2$ as a function of T/T_c in Fig. 5, which is very similar for the three models used here and which follows the values of $q_u^{\text{eff}}\sigma$, well within the error bars from the choice of the parameter τ. We have not found an explanation for this empirical law; the explored range of temperatures is too far from T_c to assume the validity of scaling laws and the density-density bulk correlation length is nearly constant and equal to σ for the SA bulk liquid over this range of temperature, while it is about 2σ for the Hg model.[21] Therefore, the result $q_u^{\text{eff}} \approx \beta\gamma_0\sigma/2$ cannot be derived from the scaling of q in terms of that correlation length as assumed in the DF analysis of Mecke and Dietrich.[12] The main correlation between the decay of $q_u^{\text{eff}}\sigma$ and other properties appears with the mean density of surface pivots, presented in Fig. 6 and discussed below. The decreasing density of the first liquid layer with increasing temperatures fits well within the classical van der Waals view of a broadening interface as T approaches T_c. The observed decrease of q_u^{eff} in our MC simulations would then be the result of an apparently stiffer intrinsic surface forced to pass through a reduced number of surface pivots. Whether or not these characteristics of our defined $\xi(\mathbf{R})$ are or not shared by the effective intrinsic surface measured by x-ray scattering would only be determined by the increasing quality of the experimental data and the careful analysis of the effective lower cutoff imposed by the detector geometry, the surface curvature, and the coherence length of the x-ray beam.[3,25,26] The ratio q_u^{eff}/q_l, determining Δ_{CW} within the CWT has often been treated as a single free parameter, drawing together the incertitudes in the lower and upper cutoffs. However, the route towards a direct experimental estimation of q_u^{eff} is open and will hopefully provide a test for the results of our computer simulations.

IV. INTRINSIC PROFILES

A. Dependence with the upper cutoff

The intrinsic profiles given by the procedure described above represent the sharpest possible atomic resolution for the interfacial structure, with a δ function to describe the position of the first liquid layer, operationally defined through the selection of the surface pivots. In our previous work[22] we showed that the two assumptions of the CWT, i.e., the statistical independence of $\tilde{\rho}(z,q_u)$ and $\xi(\mathbf{R})$, and the simple surface Hamiltonian leading to $\langle|\hat{\xi}_q|^2\rangle = (\beta\gamma_0 A_0 q^2)^{-1}$, fail when applied to the MC results with this sharpest resolution $q_u = q_m$.

The range of applicability for the CWT may be recovered by reducing the resolution of the intrinsic surface. To this effect we take an upper cutoff $q_u < q_m$ and keep in Eq. (1) only those Fourier components with $|\mathbf{q}| < q_u$ and the same values as they have for in intrinsic surface described with all the Fourier components up to q_m. Such an intrinsic surface does not go through the pivots, although it still follows their long-ranged undulations, so that the δ-function first peak in $\tilde{\rho}(z,q_m)$ becomes a Gaussian peak with increasing width as q_u decreases. The density profiles given by the full lines in Fig. 1 show how the dependence on q_u produces the gradual smoothing of the intrinsic profiles up to the plain $\rho(z,L_x)$ when q_u is pushed down to the lower cutoff $q_l = 2\pi/L_x$ set by the system size.

The same qualitative trend could be obtained keeping the maximum value of $q_u = q_m$ and defining $\xi(\mathbf{R})$ as the surface which minimizes $Q[\xi]$ in Eq. (11) with increasing values of ϵ so that this parameter would give the control of the level of molecular resolution for the intrinsic surface as a compromise between the distance to the pivots and the minimization of the area. However, the use of q_u (rather than ϵ) as a control parameter is computationally more efficient and it fits better in the established framework of the CWT.

Our prescription for $\xi(\mathbf{R})$ as a function of q_u may be changed in other aspects and hence give somewhat different shapes for $\tilde{\rho}(z,q_u)$. It appears that the simplest way to introduce the dependence on the upper cutoff would be to use $q_u = q_m$ directly as a variable, to minimize $Q[\xi]$ in Eq. (11) .

As long as these $q_u = q_m$ are around $2\pi/\sigma$ the statistical properties of the intrinsic surface and the shape of the intrinsic profiles would depend very little on the precise value of the cutoff. For $q_m \approx \pi/\sigma$, the intrinsic profiles still have a first δ-function peak, but there is an artificial increase of $|\hat{\xi}_q|^2$ typical of the overfitting requirement for the surface $\xi[\mathbf{R}]$ to pass through a number of pivots comparable to the degrees of freedom. For even lower values of $q_u = q_m$ there would be less variables in $\xi[\mathbf{R}]$ than pivots, the intrinsic surface would fail to pass over all the pivot atoms, and the intrinsic profile would take a smoother aspect similar to those obtained with our choice for $q_u < q_m$. In contrast with such piecewise behavior, our proposal to keep a fixed $q_m \approx 2\pi/\sigma$ for the selection of surface pivots and then restricting the number of Fourier components without changing their values has the advantage that both the intrinsic profiles $\tilde{\rho}(z, q_u)$ and the mean squared fluctuations of the intrinsic surface $\Delta(L_x, q_u)$ have a gradual dependence on the wave vector cutoff q_u, from the sharpest description for $q_u = q_m$ to the range of validity of the classical CWT.

B. Intrinsic profiles in normal coordinates

The intrinsic profile defined in Eq. (4) uses the macroscopic normal coordinate z to represent the distance $z_i - \xi(\mathbf{R}_i)$, between the particles and the intrinsic surface. It has been pointed out[12] that this definition should be replaced by a local normal coordinate z_n, to give a normal intrinsic profile

$$\tilde{\rho}_n(z) = \left\langle \frac{1}{A_n(z)} \sum_{i=1}^{N} \delta(z - r_i[\xi]) \right\rangle \tag{13}$$

in terms of the true distance $r_i[\xi]$ between the particle at $(\mathbf{R}_i, z_i)$ and the surface $z = \xi(\mathbf{R})$. As we already used $r_i[\xi] \leqslant \tau$ as a criterion to incorporate new pivots, we may easily compute the contributions to Eq. (13) . The main difficulty comes from the term $A_n(z)$ in the denominator, which includes the Jacobian for the transformation from $d^2\mathbf{R} = dx\, dy$ to the local transverse area, along the surface at distance z from $\xi(\mathbf{R})$. For $z = 0$, this Jacobian should just give the area of $\xi(\mathbf{R})$, i.e., $A_n(0) = A_0 + \Delta A[\xi]$, with the increase (10) over the nominal surface area $A_0 = L_x^2$, which reduces the two-dimensional density of the δ-function peak in $\tilde{\rho}_n(z)$ with respect to that in $\tilde{\rho}(z)$. However, as $|z|$ grows $A_n(z)$ should approach A_0, because the *normal* distance and the z distance would become similar. However, there is no analytic form to exactly describe the Jacobian of the transformation, which for large $|z|$ becomes a set of isolated singular points with diverging contributions.[12] To avoid this problem we have used a simple interpolation scheme

$$A_n(z) = L_x^2 \left(1 + \frac{1}{2} \sum_q \frac{|\hat{\xi}_q|^2}{(1 + |\hat{\xi}_q||z|q^2)^2} \right),$$

which gives the correction at order $1/|z|$ for a weakly corrugated surface and recovers the exact result for $z = 0$.

A normal intrinsic profile for the SA model at the triple point temperature $T/T_c = 0.12$ is presented in Fig. 7 and compared with the one obtained using the distance to the intrinsic surface along the macroscopic normal direction (4). There is a small difference in the two-dimensional density associated with the δ-function peak, since the same number of pivot atoms are divided by the macroscopic area A_0 in Eq. (4) and by the intrinsic surface area $A_n(0) = A_0 + \Delta A[\xi]$ in Eq. (13). Moreover, $\tilde{\rho}_n(z)$ shows slightly narrower and closer layers than $\tilde{\rho}(z)$ since the latter may be regarded as the average of $\tilde{\rho}_n(z)$ for different orientations of the local normal direction. The differences are reduced with $q_u < q_m$ and both intrinsic profiles recover $\rho(z, L_x)$ for $q_u = 2\pi/L_x$. For very rough surfaces, the description of the interface given by $\tilde{\rho}_n(z)$ may become qualitatively better than the description with $\tilde{\rho}(z)$, which relies on the existence of a flat macroscopic surface fixed by the boundary conditions. However, for the relatively flat interfaces explored with the slab geometries of our MC simulations, the relative increase of area $\Delta A/A_0$ is below 10% and the differences between the intrinsic representations of the interface are rather small. Moreover, the simple Gaussian convolution (5) and (6) which relates $\tilde{\rho}(z)$ with $\rho(z, L_x)$ within the CWT does not apply to $\tilde{\rho}_n(z)$, which would require a cumbersome transformation to include the inverse Jacobian from $A_n(z)$ to the macroscopic area A_0.

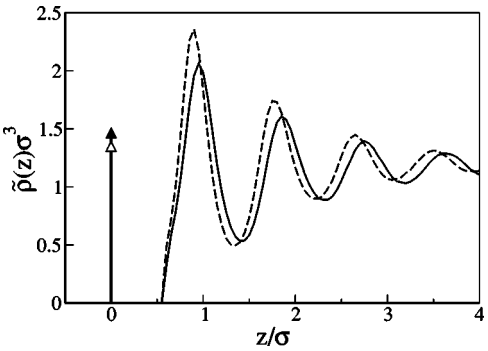

FIG. 7. The intrinsic profile for the SA model at $T/T_C = 0.12$. The full line and full vertical arrow shows the intrinsic profile obtained using the distance to the intrinsic surface along the coordinate z, $\tilde{\rho}(z, q_m)$, and the dashed line and open arrowhead give the intrinsic profile in local normal coordinates.

C. The relationship between $\tilde{\rho}(z, q_u)$ and $\rho(z, L_x)$

We turn now to the comparison between the alternative descriptions of the liquid surfaces provided by $\tilde{\rho}(z, q_u)$ and $\rho(z, L_x)$. Within the classical CWT the intrinsic profile was assumed to be essentially void of information on the microscopic structure of the interface, as the simplest step function between the densities of the coexisting vapor and liquid phases. The smooth shape of $\rho(z, L_x)$ would then be fully controlled by the function $\Delta_{\mathrm{cw}}(L_x, q_u)$, determined in Eqs. (5) and (6) by the macroscopic surface tension γ_0 and the empirical value of $q_u = 2\pi/\sigma$ (or π/σ as preferred by other authors). Alternatively, if the intrinsic profile is associated to the result of a DF approximation,[12] it would include some microscopic information, since its shape depends on the molecular interactions and T, but the effective value of q_u and

its relation to $\rho(z,L_x)$ becomes uncertain.[31] The interpretation of the x-ray reflectivity data for several liquid metals, in terms of very structured intrinsic profiles,[16,17] gave a qualitative step in the amount of microscopic information contained in $\tilde{\rho}(z,q_u)$, and partially blurred in $\rho(z,L_x)$. The Gaussian parametrization (7) uses parameters such as the occupation of the consecutive atomic layers, their relative separation, and their width, which are closer to the precise descriptions of surface reconstructions in solid interfaces than to the coarse description of a smooth density profile, typical of liquid surfaces. The MC simulations of simple fluid models with very low melting temperature[18,20] confirmed the existence of strong atomic layering in $\rho(z,L_x)$, which were well fitted by Gaussian peaks

$$\rho(z,L_x)=\sum_{i=0}^{\infty}\frac{n_i}{\sqrt{2\pi a_i}}\exp\left[-\frac{(z-z_i)^2}{2a_i}\right] \tag{14}$$

as shown by the convolution (5) and (6) of the intrinsic profile (7). The number of independent fitting parameters is reduced with constant distance between layers $z_{i+1}=z_i+\varsigma$ and constant increase of the square Gaussian width $a_{i+1}=a_i+\alpha$ for the inner layers (typically beyond $i=3$). The liquid bulk density imposes the restriction of constant occupation for the inner layers $n_i=\rho_l\varsigma$ and the values of ς and α may be related to the complex poles of the direct correlation function in the bulk liquid.[32,33] The vapor bulk density may be easily included in these description, extending the series of Gaussian peaks to the negative side of the z axis, but at low temperatures the effect is negligible in the aspect of $\tilde{\rho}(z,q_m)$.

The present analysis of the same models, with our operational definition for the intrinsic surface, enhances this view of liquid surfaces, since it increases the accuracy in the characterization of the weak layering structures observed in $\rho(z,L_x)$ and extends their study to much higher temperatures. The results for the LJ system, the prototypical model for simple fluids, show that the smooth shape of the density profile $\rho(z,L_x)$ at the triple point temperature ($T_t/T_c\approx 0.57$) hides the layering structure of the intrinsic profile $\tilde{\rho}(z,q_m)$ at its sharper level of description of the liquid surface.[22] On the other hand, the straightforward CWT relationship between $\tilde{\rho}(z,q_u)$ and $\rho(z,L_x)$ is not satisfied within our detailed view of the interfacial structure. As shown in Fig. 8, the simple Gaussian convolution (5) and (6) fails to reproduced the mean profiles $\rho(z,L_x)$ observed in our MC simulations from the intrinsic profiles $\tilde{\rho}(z,q_m)$, even if we use the mean square width Δ_{CW} (or equivalently the effective cutoff $q_u^{\rm eff}$) obtained along the same MC samplings to describe the observed width of the interface within the classical CWT. That failure implies a correlation between the intrinsic profile and the corrugations of the intrinsic surface, which were assumed negligible by the CWT.

The characterization of such correlations is better done through the fit of the intrinsic profiles $\tilde{\rho}(z,q_u)$, to the form (14) with parameters $\tilde{n}_i(q_u)$, $\tilde{z}_i(q_u)$, and $\tilde{a}_i(q_u)$, which depend on the upper wave vector cutoff q_u. The Gaussian convolution in the CWT would predict that the layer occupations and their positions should be independent of q_u, and hence equal

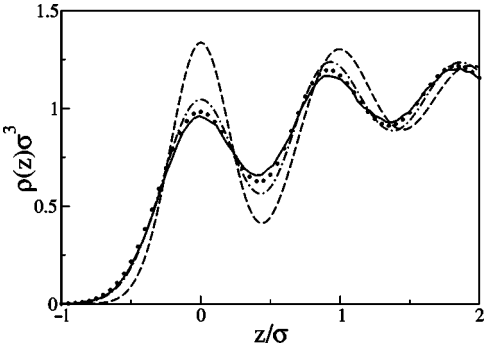

FIG. 8. The liquid-vapor density profiles $\rho(z,L_x)$, in reduced units, obtained from the simple Gaussian convolution (5) and (6) of the intrinsic profiles $\tilde{\rho}(z,q_u)$ with several values of q_u, for the SA model at $T/T_C=0.15$ and $L_x=9\sigma$. Dashed line: $q_u=\pi/2\sigma$, dashed-dotted line: $q_u=\pi/\sigma$, dotted line: $q_u=q_m$. The full line shows the mean density profile observed in our MC simulations.

to their values in the sharpest intrinsic profile (7), $\tilde{n}_i \equiv \tilde{n}_i(q_m)$ and $\tilde{z}_i \equiv \tilde{z}_i(q_m)$. The squared Gaussian widths $\tilde{a}_i(q_u)$ should be given by $\tilde{a}_i(q_m)$ incremented by the CW fluctuations $\langle|\hat{\xi}_q|^2\rangle$, added for $q_u \leqslant |\mathbf{q}| < q_m$. The independent fits of $\tilde{\rho}(z,q_u)$ are fairly compatible with common values of the layer densities $\tilde{n}_i$. They indicate a weak q_u dependence on the separation between the first layers $\tilde{z}_1-\tilde{z}_0$. However they present a clear discrepancy with the CWT prediction for the layer widths. In Fig. 9 we present the functions $\Delta_i(q_u) \equiv \tilde{a}_i(q_u)-\tilde{a}_i(q_m)$ for the first layers in the SA model at $T/T_c=0.21$ and obtained MC simulations with a large transverse size $L_x\approx 18\sigma$, which give access to values of q_u ranging from $q_l\approx 0.35/\sigma$ to $q_m\approx 6.3/\sigma$. The CWT prediction is that all these curves should be equal to the square width $\Delta_{\rm CW}(L_x,q_u)$, shown by the dashed line in the same figure. The discrepancy with such prediction is obvious and includes two different effects. The first one is that when q_u is reduced from is maximum value q_m, the increase in the width of the outer layers ($i=0,1$) is larger than the width of the intrinsic surface fluctuations for the same values of q. This effect is directly observed in the shapes of the intrinsic profiles as functions of q_u, in Fig. 1, as q_u diminishes from its maximum value q_m, the first (δ function) layer's width in-

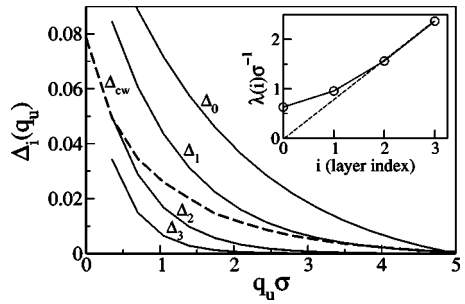

FIG. 9. $\Delta_i(q_u)=\Delta_i(q_u)\equiv\tilde{a}_i(q_u)-\tilde{a}_i(q_m)$ for the four first layers ($i=0,3$), for the SA model at $T/T_C=0.21$. The dashed line shows the CWT prediction $\Delta_{\rm CW}(L_x,q_u)$. The inset shows the parameter λ_i (circles and full line) as a function of the layer index (i), and the lineal fit of λ_i for the inner layers (dashed line).

creases rapidly without appreciable changes in the inner peaks. As q_u decreases towards $q_l = 2\pi/L_x$, the derivative of $\Delta_0(q_u)$ in Fig. 9 becomes closer to the CWT prediction, but the difference accumulated from the large q_u is reflected in the shape of $\rho(z,L_x)$ with a much wider first layer than predicted from the direct CWT convolution in Fig. 8. In our previous attempts[20] to get the intrinsic profiles as deconvolutions of $\rho(z,L_x)$ with Gaussian weights, within the CWT assumptions, we already observed that an upper cutoff $q_u = 2\pi/\sigma$ was far too short to reproduce a δ-function at the first layer of $\tilde{\rho}(z,q_u)$, as used in the interpretation of the x-ray reflectivity experiments. Our present results show that q_u^{eff} is in fact even shorter, so the relationship between the sharpest intrinsic profile $\tilde{\rho}(z,q_m)$ and the CW-averaged density profile $\rho(z,L_x)$ has to include the strong correlations between the atomic positions and the corrugations of the intrinsic surface. In particular, it is easy to observe that the positions of the pivot particles are correlated with the extrema of $\xi(\mathbf{R})$, rather than being randomly distributed over it, which may result from our definition of the intrinsic surface as the minimal area surface going through the surface pivots. It is possible that other operational definitions for the intrinsic surface might reduce these correlation effects, but if such definitions have to be pushed to the sharpest (δ-function) description of the first layer, they should also change $\gamma(q)$ to give an unphysically high effective upper cutoff $q_u^{\mathrm{eff}} \approx 4\pi/\sigma$, well beyond the resolution of atomic distances, as the only way to reproduce $\rho(z,L_x)$ within the CWT assumption. More likely we might have to accept that such a sharp resolution of the intrinsic density profile would only be possible beyond the range of validity of the classical CWT.

The second discrepancy between the CWT and our results in Fig. 9 is obvious in the square width increments of the inner layers ($i=2$ and 3). The reduction of q_u from it maximum value q_m down to half that value, produces a small increment in Δ_2, and leaves Δ_3 nearly unchanged. Only for the lowest wave vector components the inner layers seem to follow the undulations of the intrinsic surface, while the short wavelength CW modes are clearly damped in their propagation to the inner layers. From a physical point of view this is much more appealing that the CWT concept of a rigid propagation of the intrinsic profile, at a depth $z \gg \sigma$ into the bulk liquid, as consequence of a transverse modulation of wavelength $2\pi/q_m \approx \sigma$ at the surface. Such an assumption of the CWT was only made reasonable by the hypothesis of a structureless intrinsic profile, becoming constant $\tilde{\rho}(z) = \rho_l$ within one atomic diameter of the interface, so that the unphysical rigid displacement in Eq. (5) becomes irrelevant. The strong oscillations of the intrinsic profiles obtained here make the damping effect clear, and in order to quantify it we have fitted the functions in Fig. 9 as $\Delta_i(q_u) \approx \Delta_i(0) \times \exp(-\lambda_i q_u)$. For the inner layers, the parameters λ_i, shown in the inset of Fig. 9, present a linear dependence with z_i, which corresponds to a damping proportional to $\exp(-bzq)$ with a dimensionless constant b, to describe the effects of a CW with wave vector q at a depth z inside the liquid.

The enhancement due to the transverse correlations between the atoms and the extrema of $\xi(\mathbf{R})$, and the q-dependent damping of the CW effects with the depth produce opposite effects, and they may cancel each other as observed for the third layer Δ_2 at low q_u. However, a systematic exploration of these effects, either with our definition or with any other variant for the intrinsic surface, would be required for a definite answer to the relationship between $\tilde{\rho}(z,q_u)$ and $\rho(z,L_x)$ beyond the CWT prescription. Only for q_u well below the effective upper cutoff $q_u^{\mathrm{eff}}(T)$, which is itself well below $2\pi/\sigma$, could we recover the range of validity of the CWT, with intrinsic profiles $\tilde{\rho}(z,q_u)$ which are fairly smooth functions of z, keeping some weak oscillatory structure for very cold liquids ($T/T_c \leqslant 0.2$) and being monotonic at higher T/T_c. The shape of these intrinsic density profiles would depend on the choice of q_u, as well as on the temperature and the characteristics of the interactions and the CWT would correctly predict the blurring of that shape in the density profiles $\rho(z,L_x)$ for larger transverse sampling sizes.

V. CONCLUSIONS

The first conclusion we may extract from this work is that the range between the classical CWT and the description of liquid surfaces at atomic resolution, is now fully open to quantitative studies. The CWT framework currently used to interpret the experimental x-ray reflectivity data has to be extended to reach the sharpest view of the interface with atomic resolution. The computer simulations may provide a useful tool to establish a broader theoretical framework. It is well known that any thermodynamic description of curved liquid surfaces has to be based on a particular choice for the nominal mathematical surface associated to the molecular configurations.[2] The CWT predictions for long wavelength CW are independent of the particular definition for the intrinsic surface, but when we push the concept of intrinsic surface to wavelengths comparable with the atomic diameter, the surface properties should be presented and analyzed within a well characterized definition of $\xi(\mathbf{R})$.

We have checked that intrinsic surfaces defined as local Gibbs dividing surfaces[14,23] may only be used with upper wavelength cutoffs well below π/σ. Otherwise the bulk fluctuations would dominate over the surface fluctuations and produce a spurious growth of the short wavelength fluctuations of the intrinsic surface. The alternative based on the selection of surface pivots offers an operational definition which may be computed for large samplings of atomic configurations, and gives a fairly natural choice for the instantaneous location of the interface. Our proposed definition is certainly not unique but it seems to be quite robust in its predictions with respect to reasonable variants and with respect to its parameters, at least up to temperatures around the triple point of simple molecular liquids. The direct application of our definition to temperatures closer to T_c would certainly lose robustness with respect to the parameters ν and d, used for the percolation analysis previous to the selection of the surface pivots. Also the intrinsic profiles would have more artificial steps at $z=\tau$, with the parameter τ used to incorporate new pivots. These difficulties come directly from our procedure to select the first liquid layer, which may be well defined in cold liquid surfaces, but which becomes rather artificial near the critical point. Any robust definition

of $\xi(\mathbf{R})$ at high T would probably require a looser link with the atomic positions, and lead to smoother intrinsic profiles.

Our results present the cold liquid surfaces as strongly structured systems, in a trend initiated over the last decade by the analysis of x-ray reflectivity data,[16,17] reviving an old theoretical controversy on the presence of atomic layering at free liquid surfaces.[33,34] The structured intrinsic profiles extracted from the reflectivity data for some liquid metals offer a clear contrast with the stepwise shapes of $\tilde{\rho}(z)$, favored by the theoretical assumptions of the CWT, and void of any information on the surface structure. The experimental quest for layered liquid surfaces has made important advances in the quality of the experimental data and in the depth of their analysis, trying to clarify the threshold between systems with smooth density profiles, described as convolutions of stepwise intrinsic profiles with the CW distributions for the fluctuations of the intrinsic surface, and those with a structured $\tilde{\rho}(z)$, which may be recovered from behind the CW smoothing.[35]

However, the comparison of our results at the very low triple point temperature of the SA model, and those for the LJ prototype of a simple fluid, supports the idea that the atomic layering of the intrinsic surfaces is in fact a generic, and somehow trivial property of liquid surfaces, when described at the sharpest level of resolution, i.e., with a δ function to represent the density of the first atomic layer in the liquid. Such layering should be observed in liquid surfaces whenever the size of the transverse window (set by the experimental detector resolution in the x-ray experiments, or by the simulation box size L_x) becomes small enough to reduce the broadening by the CW. The surface tension, through the exponent $\eta \approx \pi/(\beta\gamma_0\sigma^2)$ in the CW damping $a(L_x) \sim L_x^{-\eta}$, for the amplitude of the density oscillations,[36] induces an effective limit of $T/T_c \approx 0.2$ for the direct observation of layering in $\rho(z,L_x)$ for the typical values ($L_x \sim 10\sigma$) used in computer simulations. For the larger sampling windows of about 1000 Å ($\approx 300\sigma$) presently used in x-ray reflectometry, the surface layering would be fully damped for $T/T_c \approx 0.15$ or higher, but this temperature threshold would be pushed up by any improvement in the experimental setup, leading to an increase in the transverse resolution.

It was already observed in the analysis of the experimental data[16,26] that the shape of the intrinsic profiles is similar to the bulk-liquid pair distribution function $g(r)$. Such an observation is confirmed by our MC results and it might appear to close the circle back to an intrinsic surface which is essentially void of information on the surface structure, since it could be inferred from the bulk liquid density and its $g(r)$, much as the simplest step function of the early CWT interpretations was fully determined by the bulk coexisting densities. Nevertheless, there are aspects of $\tilde{\rho}(z)$ which offer truly intrinsic information on the atomic structure of the surface, depending on the temperature and model interactions. The most important of these aspects is probably the two-dimensional density of the first liquid layer $\tilde{n}_0$ given by the mean number of pivot atoms per unit area, within our definition of the intrinsic surface. The results in Fig. 6 for the SA model show the decay of $\tilde{n}_0$ with increasing temperature. At the triple point temperature ($T_t/T_c = 0.12$) we find $\tilde{n}_0 \approx 0.75/\sigma^2$, while at $T/T_c = 0.66$ we get $\tilde{n}_0 \approx 0.3/\sigma^2$, although with larger error bars associated with the choice of τ. The trend is similar to our previous estimations of this layer density, from the parameter n_0 in the fit to the weakly structured density profiles $\rho(z,L_x)$, which were reduced to a shorter range of temperatures and have much larger error bars. Our previous results[19,20] from the even weaker layering observed for the Hg model, which presented an increase of n_0 with the temperature, are changed with the present and more precise estimation of $\tilde{n}_0$ into a decreasing line, parallel to that for the SA model but with denser layers at the same value of T/T_c. The results for the LJ model also run above and roughly parallel to those of the SA model, with values just above $0.5/\sigma^2$ at the triple point. The densities of the inner layers $\tilde{n}_i$, for $i \geqslant 1$, contains less information, since they rapidly converge towards the value n_b determined by the liquid bulk density and the period of the oscillations in $g(r)$. The layer width and the relative positions, as well as their correlation with the roughness of the intrinsic surface, may also contain some relevant information on the surface structure, but require further studies to discern the results from a plain convolution of the bulk liquid $g(r)$ with the structure of the first liquid layer.

The combined analysis of the specular reflectivity, the in-plane and the out-of-plane scattering of x rays from liquid surfaces[3,25,26] is providing experimental data of increasing accuracy, which are interpreted within the classical CWT framework. The reflectivity wings that are slightly out of the specular conditions are well fitted by the Gaussian fluctuations of an intrinsic surface, with the mean squared amplitude $\Delta_{\mathrm{CW}}(L_x,q_u)$ predicted by the CWT with $q_u \sim \pi/\sigma$. This is consistent with our observation of Gaussian distributions in Fig. 3, and compatible with the values of q_u^{eff} obtained in our MC simulations at low temperatures. However, our results for q_u^{off} in Fig. 5 provide effective cutoffs for the CW fluctuations which (particularly at high T) are well below the usual empirical estimations. This temperature effect on $\Delta_{\mathrm{CW}}(L_x,q_u)$ might be checked with a careful estimation of the effective sampling size L_x given by the experimental setups and the empirical law $q_u^{\mathrm{eff}} \approx \beta\gamma_0\sigma/2$, followed by our results, could be contrasted.

The recent direct experimental determinations of the q-dependent surface tension[27–29] offer a more ambitious target. The shape of $\gamma(q)$ at large q would certainly depend on the effective definition of the intrinsic surface which comes out of the experimental sampling in liquid surfaces. Hopefully, the effective $\xi(\mathbf{R})$ seen by the scattered x rays would not be very different than those obtained with our operational definition, using the most reasonable choices for the parameter τ. Nevertheless, a firm comparison between the CW observed in experiments and in simulations, as functions of their wave vector q would only be possible with a full theoretical analysis of the scattering process, going beyond the CWT assumption of uncorrelated intrinsic surfaces and intrinsic profiles. Any attempt to get a theoretical prediction for $\gamma(q)$ should also take into account the (implicit or explicit) definition used for the nominal intrinsic surface and the presence of strong correlations between the corrugations of $\xi(\mathbf{R})$ at atomic scale and the shape of the intrinsic profiles.

The effects of those correlations are even more important to extract the shape of the intrinsic profile from the experimental reflectivity data. The high quality of the present experimental data[16,17] would give a very detailed view of the intrinsic profiles, if the assumptions of the CWT were granted. However, the difference in Fig. 8, between the mean density profile $\rho(z,L_x)$ observed in our MC simulation and the CWT convolution of the sharpest intrinsic profile $\tilde{\rho}(z,q_m)$ represents a much grosser uncertainty, introduced by the correlation effects quantitatively described in Fig. 9, but fully ignored in the analysis of the experimental results. These correlations would certainly depend on the effective definition of intrinsic surface emanating from the x-ray scattering. Therefore, a thoughtful theoretical analysis of that process, together with the extension of our method to computer simulations for more realistic representations of cold liquid metal surfaces[37] seem to be the path, towards a robust characterization of those interfaces at atomic resolution. Meanwhile, the main aspect of $\tilde{\rho}(z,q_m)$ which appears to be unaffected by the correlations is the density of the first liquid layer $\tilde{n}_0$, which determines the behavior of the surface structure factor $\Phi(Q_z)$ at low Q_z. Intrinsic profiles with similar values for $\tilde{n}_i$ for all the layers, give surface structure factors increasing monotonically from a flat limit $\Phi(Q_z)=1$ at low Q_z, to a sharp peak at $Q_z \approx 2\pi/\sigma$. However, intrinsic profiles with values of $\tilde{n}_0$ well below that of the inner layers, give a function $\Phi(Q_z)$ with a shallow minima between the $\Phi(0)=1$ limit and the maximum. The comparison of the present values of $\tilde{n}_0$ for simple pairwise models, with those from computer simulations using more realistic treatments of the metallic bonding and with the experimental results for $\Phi(Q_z)$ in liquid metals may provide the first checks of the validity of the new view for liquid surfaces, described in terms of $\tilde{n}_0$, q_u^{eff}, and possibly other intrinsic parameters, which may determine the physical and chemical processes occurring on cold liquid surfaces.

ACKNOWLEDGMENTS

This work was supported by the Dirección General de Investigación, Ministerio de Ciencia y Tecnología of Spain, under Grant No. BFM2001-1679-C03.

[1] J. D. van der Waals, Verh. K. Akad. Wet. Amsterdam (Sect. 1) **1**, 56 (1893); J. Stat. Phys. **20**, 197 (1979).
[2] J. S. Rowlinson and B. Widom, *Molecular Theory of Capillarity* (Clarendon Press, Oxford, 1982).
[3] J. Penfold, Rep. Prog. Phys. **64**, 777 (2001).
[4] F. P. Buff, R. A. Lovett, and F. H. Stinger, Phys. Rev. Lett. **15**, 621 (1965).
[5] R. Evans, Adv. Phys. **28**, 143 (1979).
[6] D. Beaglehole, Phys. Rev. Lett. **43**, 2016 (1979); Physica B & C **100B**, 163 (1980).
[7] S. W. Sides, G. S. Grest, and Martin-D. Lasses, Phys. Rev. E **60**, 6708 (1999).
[8] S. Toxvaerd and J. Stecki, J. Chem. Phys. **102**, 7163 (1995).
[9] J. R. Percus, in *Fluid Interfacial Phenomena*, edited by C. A. Croxton (John Wiley, New York, 1986), pp. 1–44.
[10] S. Dietrich, J. Phys.: Condens. Matter **8**, 9127 (1996).
[11] M. Napiorkowski and S. Dietrich, Phys. Rev. E **47**, 1836 (1993).
[12] K. R. Mecke and S. Dietrich, Phys. Rev. E **59**, 6766 (1999), and references therein.
[13] A. Robledo, C. Varea and V. Romero-Ronchin, Physica A **177**, 474 (1991); V. Romero-Ronchin, C. Varea, and A. Robledo, *ibid.* **184**, 367 (1992).
[14] J. Stecki, J. Chem. Phys. **109**, 5002 (1998).
[15] A. Braslau, P. S. Pershan, G. Swislow, B. M. Ocko, and J. Als-Nielsen, Phys. Rev. A **38**, 2457 (1988); A. Braslau, M. Deutsch, P. S. Pershan, A. H. Weiss, and J. Als-Nielsen, Phys. Rev. Lett. **54**, 114 (1985).
[16] O. Magnussen, B. M. Ocko, M. J. Regan, K. Penanen, P. S. Pershan, and M. Deutsch, Phys. Rev. Lett. **74**, 4444 (1995); E. DiMasi, H. Tostmann, B. M. Ocko, P. S. Pershan, and M. Deutsch, Phys. Rev. B **58**, R13 419 (1998).
[17] M. J. Regan, E. H. Kawamoto, S. Lee, P. S. Pershan, N. Maskil, M. Deutsch, O. M. Magnussen, B. M. Ocko, and L. E. Berman, Phys. Rev. Lett. **75**, 2498 (1995).
[18] E. Chacón, M. Reinaldo-Falagán, E. Velasco, and P. Tarazona, Phys. Rev. Lett. **87**, 166101 (2001).
[19] E. Velasco, P. Tarazona, M. Reinaldo-Falagan, and E. Chacón, J. Chem. Phys. **117**, 10777 (2002).
[20] P. Tarazona, E. Chacón, M. Reinaldo-Falagan, and E. Velasco, J. Chem. Phys. **117**, 3941 (2002).
[21] P. Tarazona, E. Chacón, and E. Velasco, Mol. Phys. **101**, 1595 (2003).
[22] E. Chacón and P. Tarazona, Phys. Rev. Lett. **91**, 166103 (2003).
[23] A. Werner, F. Schmid, M. Müller, and K. Binder, J. Chem. Phys. **107**, 8175 (1997); Phys. Rev. E **59**, 728 (1999).
[24] A FORTRAN code for the computation and statistics of the intrinsic surface may be requested from the authors.
[25] J. Daillant, L. Bosio, B. Harzallah, and J. J. Benattar, J. Phys. II **1**, 149 (1991); J. Daillant and M. Alba, Rep. Prog. Phys. **63**, 1725 (2000).
[26] P. S. Pershan, Colloids Surf., A **171**, 149 (2000).
[27] C. Fradin, A. Braslau, D. Luzet, D. Smilgies, M. Alba, N. Boudet, K. Mecke, and J. Daillant, Nature (London) **403**, 871 (2000).
[28] S. Mora, J. Daillant, K. Mecke, D. Luzet, A. Braslau, M. Alba, and B. Struth, Phys. Rev. Lett. **90**, 216101 (2003).
[29] D. Li, B. Yang, B. Lin, M. Meron, J. Gebhardt, T. Graber, and S. A. Rice, Phys. Rev. Lett. **92**, 136102 (2004).
[30] A. Trokhymchuk and J. Alejandre, J. Chem. Phys. **111**, 8510 (1999).
[31] R. Checa, E. Chacón, and P. Tarazona (to be published).
[32] M. E. Fisher and B. Widom, J. Chem. Phys. **50**, 3756 (1969).
[33] R. Evans, J. R. Henderson, D. C. Hoyle, A. O. Parry, and Z. A. Sabeur, Mol. Phys. **80**, 755 (1993).
[34] C. A. Croxton and R. P. Ferrier, J. Phys. C **4**, 1909 (1971); T. R. Osborn and C. A. Croxton, Mol. Phys. **40**, 1489 (1980).

[35] O. Shpyrko, P. Huber, A. Grigoriev, P. Pershan, B. Ocko, H. Tostmann, and M. Deutsch, Phys. Rev. B **67**, 115405 (2003).
[36] R. Evans, in *Fundamentals of Inhomogeneous Fluids*, edited by D. Henderson (Dekker, New York, 1992), pp. 85–175; see also R. Evans, in *Les Houches, Session XLVIII, Liquids at Interfaces* (Elsevier, New York, 1989).
[37] D. J. González, L. E. González, and M. J. Stott, Phys. Rev. Lett. **92**, 085501 (2004).